DOI 10.1007/s10778-020-00994-z
International Applied Mechanics, Vol. 56, No. 1, January, 2020

STRESS STATE OF A THREADED JOINT IN A DENTAL IMPLANT–BONE SYSTEM*

A. Ya. Grigorenko[1], V. V. Los'[2], V. A. Malanchuk[2], and N. N. Tormakhov[1]

The load distribution over the turns of an implant–bone threaded joint is studied. Such a joint is modeled by a rod structure in which the functional axial force is transferred from the compressed-rod–implant system to the stretched-rod–bone system through thread turns. The turns are modeled by cantilever beams attached to the implant and bone rods. Differential equation describing the intensity of distribution of the axial force is derived in a closed form. The proposed approach to determining the distribution of the load over the thread of the implant–bone joint can be used to determine the stress state of the joint, improve its design, and increase the service life of dental prostheses.

Keywords: dental implant, elasticity, cortical bone, trabecular bone, thread

Introduction. The use of implants inserted in bone tissues and used as a support for dental prostheses is effective and promising trend in the field of dental orthopedics [4–6, 11–14]. Cylindrical implants with exterior thread are widely used in medical practice. An implant is mounted in a bone by preliminarily drilling a hole and screwing in. After that, an osseointegration begins, which is adherence of the bone tissue to the implant to form a single implant–bone system.

The service life of prostheses based on implants depends on the magnitude of the stresses at the implant–bone interface. For this reason, determining the stress state in the threaded implant–bone system is a topical task in stomatology and solid mechanics [2, 4, 6]. Since experimental investigations in this field either involve substantial difficulties or are impossible, the mechanical and mathematic simulation of the stress state in an implant–bone system is the basic method [2, 4, 7, 10–14].

The mechanical and mathematical simulation of the implant–bone joint is usually performed using the elasticity theory and assumptions on the geometric and mechanical characteristics of the elements of the system, their interaction conditions, and the applied loads. In [2] it was assumed that the outer surface of the implant is smooth, having no thread. The stress state of the implant–bone system was determined in [8, 9] using the spatial rod and shell models. The problem of a rod subject to a force at one end and supported by a bone as a Winkler-type foundation at the other was solved in [2]. In [10, 12], the stress–strain state of an implant–bone system was determined with the finite-element method assuming that the implant is smooth, having no thread.

The stress distribution in a threaded joint was for the first time analyzed by Zhukowsky in [3]. He assumed that the thread is square, the bolt is stretched, and the nut is compressed. The threaded joint was modeled by a structure in which the axial force is transferred from a rod (bolt) to a rod (nut) through thread turns in the form of cantilever beams. In accordance with Zhukowsky's model, the turns undergo only shear strains. The forces transferred by the turns are determined as the sum of an infinite geometrical progression. Zhukowsky showed that, the forces in the turns of the threaded joint are distributed

[1]S. P. Timoshenko Institute of Mechanics, National Academy of Sciences of Ukraine, 3 Nesterova Str., Kyiv, Ukraine 03057; e-mail: ayagrigorenko1991@gmail.com. [2]Bogomolets National Medical University, 34 Pobedy Av., Kyiv, Ukraine 03057; e-mail: losvmail@gmail.com. Translated from Prikladnaya Mekhanika, Vol. 56, No. 1, pp. 44–51, January–February 2020. Original article submitted November 21, 2018.

* This study was sponsored by the budgetary program Support of Priority Areas of Research (KPKVK 6541230).

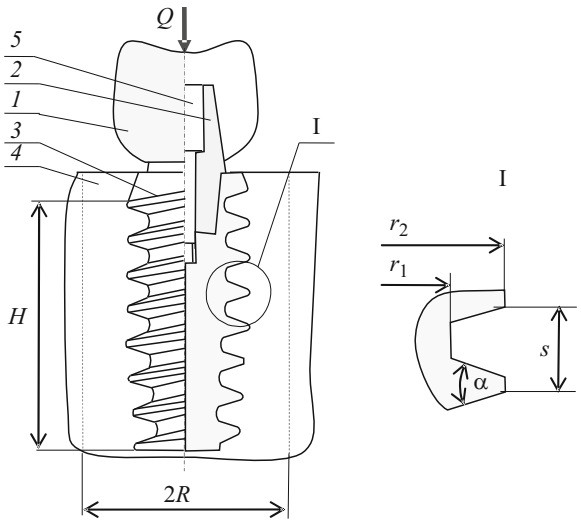

Fig. 1

TABLE 1

Material	*E*, GPa	μ
Compact bone	13.7	0.30
Trabecular bone	6.9	0.30
Titan alloy VT1-100	111.0	0.35

nonuniformly, and the distribution depends on the geometrical parameters of the threaded joint and the stiffness of the bolt and the nut.

Later on, Zhukowsky's model was developed in [1], where a threaded joint with triangular turns undergoing shear, bending, and transverse strains was addressed. It was assumed that the joint has continuous turns, making it possible to employ differential equations solved in closed form. Two types of threaded joint were considered: in first-type joint, the bolt is stretched while the nut is compressed; in the second-type joint (brace) both bolt and nut are stretched.

The stress state of a threaded implant–bone joint in which the implant is stretched while the bone tissue is compressed was considered in [4] where the joint was assumed to be a statically indeterminate frame structure. The distribution of forces between turns of the threaded joint was determined by the methods of structural mechanics.

It should be noted that the loading configuration [4] where the implant is stretched while the bone tissue is compressed is rare in stomatology. The functional forces exerted by the bolus compress the implant and stretch the adjoining bone tissue. Such a loading configuration is addressed here. To describe the distribution of the functional load over the thread turns, we will employ the approach from [1].

Our goal here is to develop a technique for determining the distribution of the load over the turns of the threaded implant–bone joint to improve the implant design and increase the service life of associated prostheses.

1. Prosthesis Design Based on Screw-Threaded Implants. Figure 1 shows a typical prosthesis comprising artificial dental crown *1*, abatement *2*, implant *3* in bone tissue *4*, and screw *5* attaching the abatement to the implant. The vertical functional load *Q* acts on crown *1* and is transferred through abatement *2* and implant *3* to bone tissue *4*. The bone has outer cortical and inner trabecular layers. The cortical or compact bone has a dense homogeneous structure, while the trabecular one has a porous structure penetrated by blood vessels. The implant can be inserted either in the cortical bone or in the trabecular one. Table 1 presents the elastic moduli *E* and Poisson ratios μ of the cortical and trabecular bones as well as of the titan alloy the

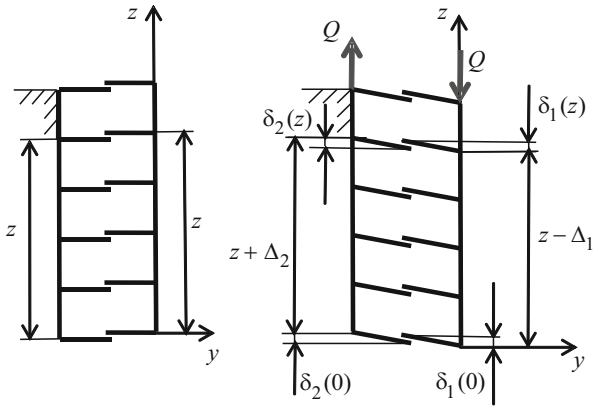

a *b*

Fig. 2

implants are made of. As is seen, the elastic modulus and strength of the compact bone are almost twice as high as those for the trabecular bone and substantially lower than those of VT1-100 titan alloy.

2. Compatibility Equations for the Displacements of the Implant and Bone. The design model of a threaded implant–bone joint before and after loading by the force Q is shown in Figs. 2*a* and 2*b*, respectively.

The functional load is transferred from the implant to the bone through the threaded joint causing compression of the implant and tension of the adjacent bone tissue. The force in the implant and bone varies from 0 to Q, becoming $Q(z)$ at a distance z from the coordinate origin.

Assume that the force $Q(z)$ generates a normal stress $\sigma_1(z)$ that is uniformly distributed over the implant cross-section but varies along the z-axis as

$$\sigma_1(z) = \frac{Q(z)}{F_1}, \tag{1}$$

where $F_1 = \pi r_1^2$ is the implant cross-sectional area, r_1 is the inner radius of the implant thread.

Let us isolate a zone of the bone tissue adjacent to the implant in the form of a hollow cylinder with outer and inner radii R and r_2, respectively. Let the cross-sectional area be acted upon by the uniformly distributed normal stress

$$\sigma_2(z) = \frac{Q(z)}{F_2}, \tag{2}$$

where $F_2 = \pi(R^2 - r_2^2)$ is the cross-sectional area of the tissue zone adjacent to the bone. Under the load Q, the implant shortens on the segment from 0 to z by Δ_1 while the bone tissue elongates by Δ_2 as follows:

$$\Delta_1 = \int_0^z \frac{\sigma_1(z)}{E_1}\,dz = \int_0^z \frac{Q(z)}{E_1 F_1}\,dz,$$

$$\Delta_2 = \int_0^z \frac{\sigma_2(z)}{E_2}\,dz = \int_0^z \frac{Q(z)}{E_2 F_2}\,dz. \tag{3}$$

The points of the thread turns of the implant and bone that lie on the effective diameter of the thread and at the distance $z = 0$ shift by $\delta_1(0)$ and $\delta_2(0)$ in the axial direction as a result of bending, shear, and transverse deformation of the turns under the action of the axial force Q. The same points located at the distance z from the coordinate origin shift by $\delta_1(z)$ and $\delta_2(z)$.

Let the contact pressure $p(z)$ be uniformly distributed over the surface of the thread turn and dependent on z only. Let us express the shifts $\delta_1(z)$ and $\delta_2(z)$ in terms of the contact pressure $p(z)$, thread pitch s, elastic moduli E_1 and E_2, and the dimensionless coefficients λ_1, λ_2 as follows [1]:

$$\delta_1(z) = \frac{p(z)s\lambda_1}{E_1},$$

$$\delta_2(z) = \frac{p(z)s\lambda_2}{E_2}. \tag{4}$$

The coefficients λ_1 and λ_2 depend on the geometry of the threaded joint and are defined as follows [1]:

$$\lambda_1 = \omega + \frac{r_1 t}{s^2}(1-\mu_1)\tan^2\frac{\alpha}{2},$$

$$\lambda_2 = \omega + \frac{r_2 t}{s^2}\left(\frac{R^2 + r_2^2}{R^2 - r_2^2} + \mu_2\right)\tan^2\frac{\alpha}{2}, \tag{5}$$

where $\omega = 0.84$ is a coefficient characterizing the bending and shear of a turn; $t = r_2 - r_1$ is the thread height; α is the thread angle.

Based on Fig. 2, we can write the compatibility equation for the displacements of the screw and nut and the displacements of the thread turns:

$$z - \Delta_1 - \delta_1(0) + \delta_1(z) = z + \Delta_2 + \delta_2(0) - \delta_2(z). \tag{6}$$

Transforming this equation and considering (4) and (5), we obtain

$$\left(\frac{1}{E_1F_1} + \frac{1}{E_2F_2}\right)\int_0^z Q(z)\,dz = [p(z) - p(0)]\left(\frac{\lambda_1}{E_1} + \frac{\lambda_2}{E_2}\right)s. \tag{7}$$

Let us introduce the intensity of the distribution of the axial force over the length $q(z)$ of the threaded joint:

$$q(z) = \frac{dQ}{dz}, \tag{8}$$

which is related to the pressure $p(z)$ on the turn surface as

$$p(z) = q(z)\frac{f}{s}, \tag{9}$$

where $f = \pi(r_2^2 - r_1^2)$ is the projection of the thread turn onto a plane perpendicular to the implant axis. Substituting $q(z)$ for $p(z)$ into (7), we get

$$\left(\frac{1}{E_1F_1} + \frac{1}{E_2F_2}\right)\int_0^z Q(z)\,dz = [q(z) - q(0)]\left(\frac{\lambda_1}{E_1} + \frac{\lambda_2}{E_2}\right)\frac{s^2}{f}. \tag{10}$$

Let

$$\beta = \frac{1}{E_1F_1} + \frac{1}{E_2F_2}, \qquad \gamma = \left(\frac{\lambda_1}{E_1} - \frac{\lambda_2}{E_2}\right)\frac{s^2}{f}. \tag{11}$$

Then Eq. (10) becomes

$$\int_0^z Q(z)\,dz = [q(z) - q(0)]\gamma. \tag{12}$$

Differentiating (12) with respect to z, we obtain

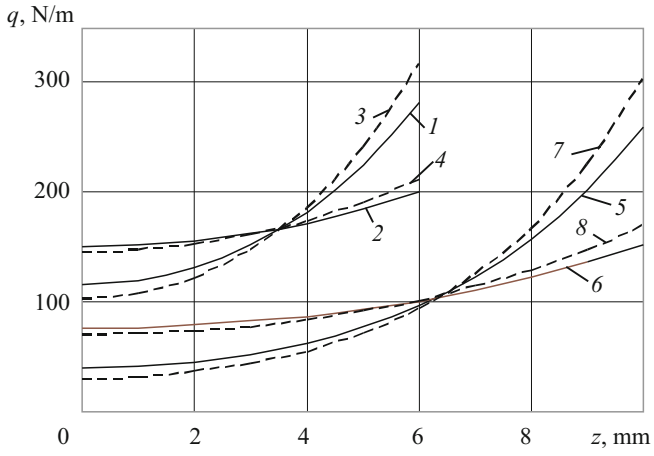

Fig. 3

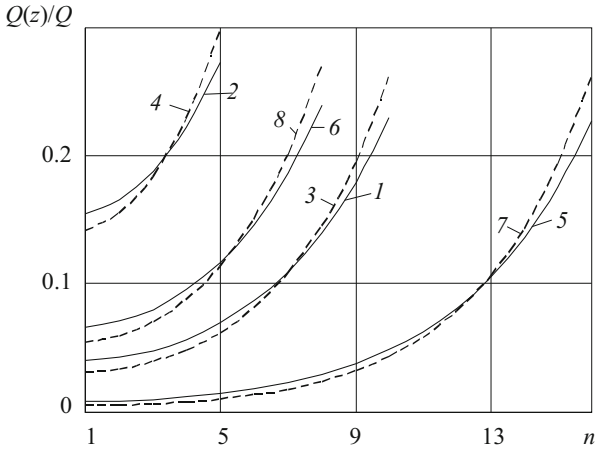

Fig. 4

$$\beta Q(z) = q'(z)\gamma. \tag{13}$$

Repeating differentiation of (13) with respect to z and denoting $m^2 = \beta / \gamma$, we find

$$q''(z) - m^2 q(z) = 0. \tag{14}$$

The general integral of Eq. (14) takes the form

$$q(z) = A\sinh(mz) + B\cosh(mz). \tag{15}$$

This equation must satisfy the following boundary conditions:

at $z = 0$

$$Q(0) = 0, \qquad q'(z) = m^2 Q(0) = 0,$$

at $z = H$ (H is the implant length)

$$Q(H) = Q, \qquad q'(z) = m^2 Q(H) = m^2 Q.$$

From (15) it follows that

$$q'(z) = Am\cosh(mz) - Bm\sinh(mz). \tag{16}$$

Then, using the boundary conditions, we get

$$A = 0, \qquad B = \frac{Qm}{\sinh(mH)}. \tag{17}$$

Substituting the values of the constants A and B into (15) yields

$$q(z) = -\frac{Qm\cosh(mz)}{\sinh(mH)}. \tag{18}$$

According to (13), the force $Q(z)$ in the implant is defined by

$$Q(z) = \frac{Q\sinh(mz)}{\sinh(mH)}. \tag{19}$$

TABLE 2

No.	H, mm	E_2, GPa	s, mm	n, turns	m, m^{-1}	ΔQ, %
1	10	13.7	1	10	256.8	23.0
2	10	13.7	2	5	131.1	27.2
3	10	6.9	1	10	300.0	26.1
4	10	6.9	2	5	153.8	29.5
5	16	13.7	1	16	256.8	22.7
6	16	13.7	2	8	131.1	23.9
7	16	6.9	1	16	300.0	25.9
8	16	6.9	2	8	153.8	26.9

Figures 3 and 4 show how the intensity $q(z)$ varies along the length of the threaded joint and the axial force $Q(z)$ varies along the thread turns, respectively. Both graphs were plotted using (18) and (19). It is assumed that Q = 1 N. Eight cases summarized in Table 2 were considered. The results were obtained for cortical (E_2 = 13.7 GPa) and trabecular (E_2 = 6.9 GPa) bones and titan implant with thread parameters $r_1 = 2.1$ mm, $r_2 = 2.5$ mm, $\alpha = 30^{\circ}$. Since the volume of the jaw bone is limited across the thickness, the outer diameter of the bone zone acted upon by the functional load is greater by 2 mm than the outer diameter of the thread, i.e., $R = 2 + r_2$. It was assumed that the implant length H is equal to 10 and 16 mm, and the thread pitch s is equal to 1 and 2 mm. The number n of turns in the joint varied from 5 to 16.

The dashed curves in Figs. 3 and 4 represent the cortical bone, while the solid curves, the trabecular bone. As is seen, the behavior of the forces $q(z)$ and $Q(z)$ strongly depends on the geometrical parameters H and s of the joint. The difference between the functions $q(z)$ and $Q(z)$ in the range of variation in H and s exceeds 100%. The distribution of the load over the thread turns in the implant–trabecular bone system is more nonuniform than in the implant–cortical bone system. The differences of the functions $q(z)$ and $Q(z)$ between these bone tissues reaches 12%. The maximum intensity of distributions of the axial forces $q(z)$ and $Q(z)$ and of the force ΔQ applied to the single turn is observed at the point of application of the compressive force $z = H$ to the implant.

The values of the parameter m and maximum axial force ΔQ (in percent of Q) taken up by the thread turn that has the coordinate z in the interval from $(H - s)$ to H are given in the next-to-last and last columns of Table 2. Analyzing Figs. 3 and 4 and Table 2, we can conclude that ΔQ increases with increasing thread pitch s and decreasing implant length H and bone elastic modulus E_2. For case 4 (an implant with thread pitch s = 2 mm and length H = 10 mm in the trabecular bone), the maximally loaded turn bears 29.5% of the axial force Q.

Conclusions. The physiological and aesthetic functions of patients with defects in the dental arch are recovered using prostheses based on dental implants. The motion of the low jaw while chewing a bolus gives rise to functional loads that act through the prosthesis on the implants and, in case of overloading, may result in necrosis and falling out of implants. The action of the functional load in the implant–bone system acting along the implant axis has been analyzed. The deformation of the implant and adjacent bone tissue causes nonuniformity of the distribution of the load between turns of the threaded implant–bone joint. The thread turn that is the closest to the point of application of the load is maximally loaded. It has been established that the distribution of the axial load depends on the length and pitch of the implant thread. Moreover, the distribution of the load over the thread turns depends on the stiffness of the bone tissue and the mechanical properties of the implant. It has been shown that the distribution of the load over the turns in the implant–cortical bone system is more uniform than in the implant–trabecular bone system. The difference between the maximum forces for these types of joint in the case of implants made of titan alloy does not exceed 12%.

REFERENCES

1. I. A. Birger and G. B. Iosilevich, *Threaded and Flange Joints* [in Russian], Mashinostroenie, Moscow (1990).
2. Ya. M. Grigorenko, V. V. Los', and A. T. Vasilenko, "Stress state analysis of the implant–bone system in teeth prosthetics," *Dop. NAN Ukrainy*, No. 3, 177–183 (2004).
3. N. E. Zhukowsky, "Distribution of pressures on the threads of a screw and nut," *Byul. Polytekhn. Obshch.*, No. 1, 50–54 (1902).
4. A. N. Chuiko et al., *Biomechanics and Computer Technologies in Maxillofacial Surgery and Dental Implantology* [in Russian], GalDent, Lviv (2014).
5. M. Daas, G. Dubois, A. S. Bonnet, P. Lipinski, and C. Rignon-Bret, "A complete finite element model of a mandibular implant-retained overdenture with two implants: Comparison between rigid and resilient attachment configurations," *Medical Eng. Phys.*, **30**, 218–225 (2008).
6. A. N. Natali (ed.), *Dental Biomeechanics*, Tailor & Francis, London (2003).
7. A. Ya. Grigorenko, E. N. Pliska, G. V. Sorochenko, and N. N. Tormachov, "Application of methods of numerical analysis for studying mechanical processes in biomechanics," *Int. Appl. Mech.*, **54**, No. 3, 366–372 (2018).
8. Ya. M. Grigorenko and L. S. Rozhok, "Layered inhomogeneous hollow cylinders with concave corrugations under internal pressure," *Int. Appl. Mech.*, **54**, No. 5, 531–538 (2018).
9. A. Ya. Grigorenko, N. P. Yaremchenko, and S. N. Yaremchenko, "Analysis of the axisymmetric stress–strain state of a continuously inhomogeneous hollow sphere," *Int. Appl. Mech.*, **54**, No. 5, 577–583 (2018).
10. Y. M. Huang, I. C. Chou, C. P. Jiang, Y. S. Wu, and S. Y. Lee, "FE analysis of dental implant neck effects on primary stability and osseointegration in a type IV bone mandible," *Biomed Mater. Eng.*, **24**, No. 1, 1407–1415 (2014).
11. J. S. Lee, I. H. Cho, Y. S. Kim, S. J. Heo, H. B. Kwon, and Y. J. Lim, "Bone–implant interface with simulated insertion stress around an immediately loaded dental implant in the anterior maxilla: a three-dimensional finite element analysis," *Int. J. Oral Maxillofac Implants*, **27**, No. 2, 295–302 (2012).
12. G. Limbert, C. Lierde, O. L. Muraru, et al., "A micro-CT-based three-dimensional finite element study," *J. Biomech.*, **43**, 1251–1261 (2010).
13. C. Vanegas-Acosta, N. S. Landinez, D. A. Garzon-Alvarado, and M. C. Casale, "A finite element method approach for the mechanobiological modeling of the osseointegration of a dental implant," *Comput. Methods Programs Biomed*, **101**, No. 3, 297–314 (2011).
14. W. Winter, P. Steinmann, S. Holst, and M. Karl, "Effect of geometric parameters on finite element analysis of bone loading caused by nonpassively fitting implant-supported dental restorations," *Quintessence Int.*, **42**, No. 6, 471–478 (2011).